J Biol Inorg Chem (2006) 11:891–902
DOI 10.1007/s00775-006-0142-5

ORIGINAL PAPER

The crystal structure of *Deinococcus radiodurans* Dps protein (DR2263) reveals the presence of a novel metal centre in the N terminus

Célia V. Romão · Edward P. Mitchell · Sean McSweeney

Received: 27 April 2006 / Accepted: 26 June 2006 / Published online: 20 July 2006

Abstract The crystal structure of a DNA-binding protein from starved cells (Dps) (DR2263) from *Deinococcus radiodurans* was determined in two states: a native form, to 1.1-Å resolution, and one soaked in an iron solution, to 1.6-Å resolution. In comparison with other Dps proteins, DR2263 has an extended N-terminal extension, in both structures presented here, a novel metal binding site was identified in this N-terminal extension and was assigned to bound zinc. The zinc is tetrahedrally coordinated and the ligands, that belong to the N-terminal extension, are two histidines, one glutamate and one aspartate residue, which are unique to this protein within the Dps family. In the iron-soaked crystal structure, a total of three iron sites per monomer were found: one site corresponds to the ferroxidase centre with structural similarities to those found in other Dps family members; the two other sites are located on the two different threefold axes corresponding to small pores in the Dps sphere, which may possibly form the entrance and exit channels for iron storage.

Keywords Crystallization · DNA-binding protein from starved cells · Iron · *Deinococcus radiodurans*

Introduction

Deinococcus radiodurans is an aerobic bacterium extremely resistant to a wide range of agents and conditions that damage DNA, including desiccation and ionising and ultraviolet radiation [1, 2]. Despite much recent research that has been carried out on this bacterium and all the hypotheses proposed, the mechanisms underlying the radiation resistance are not fully understood. A relationship between the differences in resistance to γ-radiation and desiccation for different bacteria has been proposed to be correlated with their intracellular Mn/Fe concentration [3, 4]. *D. radiodurans* is known to accumulate high intracellular manganese and to maintain low iron levels [3, 4]. In the *D. radiodurans* genome [1] there is no gene coding for a ferritin-type iron-storage protein, indicating therefore that iron may not have an essential role in this organism. However, there are two genes encoding for putative DNA-binding proteins, DNA-binding protein from starved cells (Dps), homologous to the *Escherichia coli* protein [5, 6]. One of the Dps genes is encoded on chromosome 1, corresponding to DR2263, whilst the other, DRB0092, is encoded on megaplasmid MP1 [1]. These two proteins may function as iron-storage proteins and at the same time protect the DNA from oxidative stress conditions.

Dps are a family of prokaryotic proteins associated with oxidative stress response, being able to protect DNA under those conditions presumably by suppression of Fenton chemistry. Crystallographic studies on these proteins have revealed a structural similarity to the iron-storage ferritin family. Dps and ferritins share a hollow spherical structure, but with only 12 subunits instead of 24 subunits. The Dps dodecamers have an external and internal diameter of approximately 90 and 45 Å, respectively. Each subunit is a four-helix bundle with a short helix in the middle of the BC loop and the 12 subunits assemble with 23 symmetry [6–15].

C. V. Romão · E. P. Mitchell · S. McSweeney (✉)
European Synchrotron Radiation Facility,
BP-220, 38043 Grenoble Cedex, France
e-mail: mcsweeney@esrf.fr

Although all the members of the Dps family share the same dodecameric structure they have different proposed functions. They can act as iron-storage proteins with two intersubunit ferroxidase centres for iron oxidation, having the capacity to incorporate up to 500 iron atoms [16–18]. The amino acid residues forming the ferroxidase iron binding site are contributed by both of the symmetry-related monomers and are quite conserved amongst members of the Dps family known to date. In some of the published crystal structures, it was possible to observe iron bound at this site [7, 9–15]. Mutations of residues involved in this intersubunit site for the Dps-like peroxide resistance protein (Dpr) in *Streptococcus suis* resulted in a considerable decrease in iron incorporation in vivo [19]. However, there are examples of Dps family members that do not have these residues, such as DpsA and DpsB from *Lactococcus lactis*, which both lack the conventional ferroxidase centre [8] and for the Dps-like protein from archaeon *Sulfolobus solfataricus*, which is able to catalyse iron oxidation, for which the sequence alignment within the monophyletic cluster suggested a different metal binding motif potentially involved in iron coordination: His/Gln$(X)_{13}$Glu$(X)_{10}$ Glu/Gln$(X)_7$Glu [20].

Some members of the Dps family bind DNA without any apparent sequence specificity, and they protect the DNA from damage as a result of oxidative stress. The *E. coli* Dps is upregulated under stress and induces the formation of toroidal assemblies of chromosomal DNA in such a way that the DNA molecules are physically sequestered and structurally protected [21, 22]. The DNA interaction mechanism is not yet completely established. For *E. coli* Dps it has been proposed to be associated with the presence of a lysine-containing N-terminal extension; the motif contains three lysines residues and is Lys5$(X)_2$Lys8(X)Lys10, presumably by extending away from the compact sphere into the solvent, thereby interacting with the DNA strands [6, 23]. In the case of *Mycobacterium smegmatis* Dps, DNA interaction is proposed to be related to the presence of positive residues (mainly lysines and arginines) located on the C-terminal which may be able to facilitate interactions with DNA [15]. Recently it was shown that for *Lac. lactis* DpsA the N-terminal region is required for DNA binding, although the positively charged lysine residues within this region are not essential for mediating DNA interactions [8]. In fact, crystal structures of both DpsA and DpsB from *Lac. lactis* show an N-terminal extension forming a helix extending perpendicularly away from the protein, exposed on the dodecamer surface and being available to interact with DNA [8].

There are examples of Dps having a dual function: they can interact with DNA and sequester iron by protecting DNA from oxidative damage, by acting as a physical shield and by inhibiting Fenton chemistry [4, 5, 15, 24].

The two only organisms which contain two different genes encoding for Dps-like proteins are the bacterium *Bacillus anthracis* [12], with Dlp-1 and Dlp-2, and the radiation-resistant bacterium *D. radiodurans*, with DR2263 and DRB0092. In both bacteria the cellular functions of the two different Dps are unknown. In the case of *D. radiodurans*, from an analysis of a transcriptome dynamics study, the profile for expression levels of both proteins could not clarify the roles of either protein [25]. Recently, it was shown that Dps DR2263 binds DNA, both in dimeric and dodecameric forms of the protein, and it was proposed that each of the Dps DR2263 forms has different functions: both forms exhibit ferroxidase activity, but only the dimeric form protects DNA from hydroxyl radicals [26]. Thus, the cellular function and the roles associated with radiation recovery remain to be elucidated for both Dps from *D. radiodurans*. The crystal structures of Dps DR2263 presented in this paper suggest a possible role in iron oxidation and also in DNA binding for this protein.

Materials and methods

Cloning, expression and purification of Dps DR2263 from *D. radiodurans*

The gene encoding Dps DR2263 was amplified from *D. radiodurans* R1 genomic DNA using the Gateway System (Invitrogen) with the donor vector pDNOR221 and the destination vector pDest14. Both forward and reverse primers were designed in accordance with the system. The resulting plasmid was transform into *E. coli* BL-21 (DE3). Overexpression was obtained by growing cells at 37 °C in Luria–Bertani medium containing ampicilin (100 μg/ml) to an optical density at 600 nm of 0.7–0.8 which were then induced with 1 mM of isopropyl β-D-thiogalactopyranoside and grown overnight at 20 °C. The cells were harvested and resuspended into 10 mM tris(hydroxymethyl)aminomethane (Tris)–HCl, pH 7.5 and broken in a French Press pressure cell (Stansted) at 9,000 psi. The overexpressed protein was found in inclusion bodies, which were collected along with other cell debris by low-speed centrifugation at 5,000*g* for 10 min. The suspension was dissolved in solubilisation buffer, 8 ml/g, 20 mM Tris–HCl pH 7.5, 8 M urea, 0.5 M NaCl, 5 mM

DTT, and stirred at room temperature for 30 min. Insoluble material was eliminated by centrifugation at 17,000*g*, for 15 min. The supernatant was then dialysed, firstly with 1 l urea (8 M) for 2 h, then eight times 250 ml 25 mM Tris–HCl pH 7.5, 150 mM NaCl was added in time intervals of 2 h. The sample was then dialysed against 2 l of 25 mM Tris–HCl (pH 7.5, 150 mM NaCl) and finally against 25 mM Tris–HCl pH 7.5. The solution was centrifuged (15,000*g*, 20 min) and the supernatant loaded on an ionic exchange 5-ml Hi-Trap HP column (2 ml/min 20 mM Tris–HCl pH 7.5, 1 M NaCl). The Dps DR2263 sample was eluted at 300 mM NaCl, concentrated using an Amicon-Ultra centrifugal filter and finally applied on to a Superdex S-200 XK16/60 (0.8 ml/min, 20 mM Tris–HCl pH 7.5, 150 mM NaCl). The protein obtained was pure as judged by sodium dodecyl sulphate polyacrylamide gel electrophoresis analysis. The N-terminal sequence was confirmed by Edman degradation performed by the sequence service of the Institut de Biologie Structurale, Grenoble, France.

Protein crystallisation and soaking

Crystallisation conditions were screened using the nanodrop crystallisation robot of the Partnership for Structural Biology—High Throughput Crystallisation Platform (EMBL, Grenoble). Crystals were obtained at 20 °C in 200 mM lithium sulphate monohydrate, 100 mM Tris–HCl pH 8.5, 15% poly(ethylene glycol) 4000. Crystal A was crystallised by the hanging-drop method by mixing 2.0 µl of native protein as purified (8 mg/ml) with 2.0 µl of reservoir solution. Crystal B corresponds to native protein crystallised with a protein concentration of 13 mg/ml and the resulting crystals were soaked in 10 mM ferrous ammonium sulphate solution for 15 min.

X-ray data collection and processing

Crystal A was cryo-protected with a solution of 25% glycerol in the mother liquor and crystal B was cryo-protected with a solution of 30% glycerol in the mother liquor. Both crystals belong to the cubic space group *P*23 with unit cell dimensions of $a = 90.39$ Å for crystal A and 90.2 Å for crystal B, and a Matthews coefficient V_m of 2.7 Å^3/Da, corresponding to an estimated 53% solvent content and one monomer in the asymmetric unit.

Diffraction data were collected using X-rays of wavelength of 0.933 Å at the European Synchroton Radiation Facility on beamline ID14-1 using an ADSC Q4 CCD detector to 1.1- and 1.6-Å resolution for crystals A and B, respectively. Highly redundant data were collected from crystal B in order to allow structure determination by using the remote single-wavelength anomalous diffraction (SAD) technique. Both datasets were integrated using MOSFLM [27] and scaled, merged and converted to structure factors with SCALA and TRUNCATE [28, 29]. The statistics of each dataset are presented in Table 1.

Phasing and refinement of the structures

The structures were determined using the data from crystal B. The anomalous Patterson maps generated from the highly redundant data suggested the presence of three metal sites; autoSHARP [30] was therefore directed to search for three sites per monomer. The phases from autoSHARP were transferred to the data collected from crystal A. Both structures were constructed independently using arpWARP [31], resulting in initial models of 163 residues and 175 residues, out of a total of 207 possible, for structures A and B, respectively. Refinement for both structures was carried out using cycles of REFMAC [32] and manual reconstruction with O [33]. For structure A, anisotropic *B* factors were refined on all the atoms; for structure B significant deviation was observed from spherical electron density for the metals and so anisotropic *B* factors were applied to the metal sites. Water

Table 1 X-ray data-processing statistics for DNA-binding protein from starved cells (*Dps*) DR2263

	Structure A, native	Structure B, iron-soaked
Beamline	ID14-1 (ESRF)	ID14-1 (ESRF)
Wavelength (Å)	0.933	0.933
Temperature (K)	100	100
Space group	*P*23	*P*23
Unit cell (Å)	90.39	90.2
Resolution (Å)	21.31–1.10 (1.13–1.10)	31.91–1.60 (1.64–1.60)
R_{merge} (%)	6.3 (47.7)	9.4 (56.9)
$I/\sigma(I)$	13.7 (2.5)	56.5 (11.1)
Wilson *B* factor (Å^2)	6.3	13.6
Completeness (%)	99.6 (98.1)	100.0 (100.0)
Redundancy	5.4 (3.9)	84.0 (84.7)
Number of observations	537,021 (27,689)	2,736,421 (202,055)
Number of unique reflections	99,021 (7,138)	32,579 (2,386)
Phasing power	–	0.91
R_{cullis}	–	0.849
Figure of merit before solvent flattening	–	0.31

Numbers in *parentheses* refer to the highest-resolution shell

ESRF European Synchroton Radiation Facility

molecules were placed automatically with REFMAC and arpWARP. On both structures presented here, native form and iron-soaked, the first 29 amino acid residues could not be located in the electron density and therefore were not modelled.

For both structures A and B, the electron density maps revealed the presence of an unsuspected strongly bound metal ion located in the N-terminal extension. The identity of the ion as Zn was verified with diffraction data collected (statistics not shown) above and below the Zn K-absorption edge on ESRF beamline ID23 with crystals of type A (native). Phased anomalous maps using calculated phases from the final native model show a peak of 43.0σ above the edge and a peak of 4.0σ below the edge at the Zn position.

For both structures A and B phased anomalous maps were calculated using the data collected at 0.933-Å wavelength. Besides the zinc site in the N-terminal extension found in both structures, only one other peak (7.6σ) was observed for structure A; whilst for structure B three peaks (49.7σ, 34.4σ and 19.1σ) were observed. In order to assess the relative occupancy of the metal sites, these sites were refined with various occupancies in an attempt to match the site *B* factor with those of the surrounding ligands. For structure A, the zinc site was finally refined at 75% occupancy and the 7.6σ peak (threefold C-terminal pore) was refined at 45% occupancy. For structure B, the zinc site was refined at 100% occupancy and the other peaks were refined: 49.7σ peak (intersubunit ferroxidase centre) at 100% occupancy, the 34.4σ peak (threefold N-terminal pore) at 84% occupancy and the 19.1σ peak (threefold C-terminal pore) at 84% occupancy.

The refinement statistics of each structure are presented in Table 2. The Ramachandran plot shows no residues in the disallowed regions for both structures. All the stereochemical criteria as calculated by PROCHECK [34] satisfy or are better than the average values structures determined at a similar resolution. The overall *G* factor is 0.2 for both structures A and B.

Sequence alignment

Multiple amino acid sequence alignment was made with Dps or Dps-like sequences where crystal structures had been published, using Clustal W [35], and were readjusted using Genedoc [36] based on structural alignments made using the SwissPDB [37].

Figures

Figures 1a and b, 3b, 4 and 5a and b were prepared with MolScript [38] and Raster3D [39]. Figure 3a was prepared with BobScript [40] and Raster 3D [39].

Table 2 Refinement statistics for Dps DR2263

	Structure A, native 1.1 Å	Structure B, iron-soaked 1.6 Å
R (%) (no. of reflections)	12.6 (94,077)	13.1 (30,939)
R_{free} (%) (no. of reflections)	14.8 (4,931)	15.3 (1,638)
Average *B* factors	11.3	14.8
Root-mean-square deviations from standard geometry (Å)		
Bond lengths	0.019	0.020
Bond angles	1.702	1.637
Bond torsions	4.821	4.844
Number of non-hydrogen atoms		
All	1,856	1,774
Protein	1,505	1,463
Water	344	278
Fe	1	3
Zn	1	1
Sulphate	5	5
Glycerol	0	24
Residues with two conformations	Glu54, Glu100, Glu110, Glu114, Glu141, Arg92, Arg205, Leu96, Asp99, Asp172, Asp181, Thr135, Pro139, Lys192	Leu66, Leu96, Leu124, Arg92, Ala125, Thr135, Gln137, Asp172
Residues with three conformations	Glu104, Arg159	Arg159
B factor (*B* factor average for the ligands)		
Zn (N-terminal extension)	7.25 (9.42)	14.5 (14.4)
Fe (ferroxidase centre)	–	7.7 (7.4)
Fe (threefold N-terminal pore)	–	7.7 (17.2)
Fe (threefold C-terminal pore)	8.6 (17.6)	19.4 (20.5)

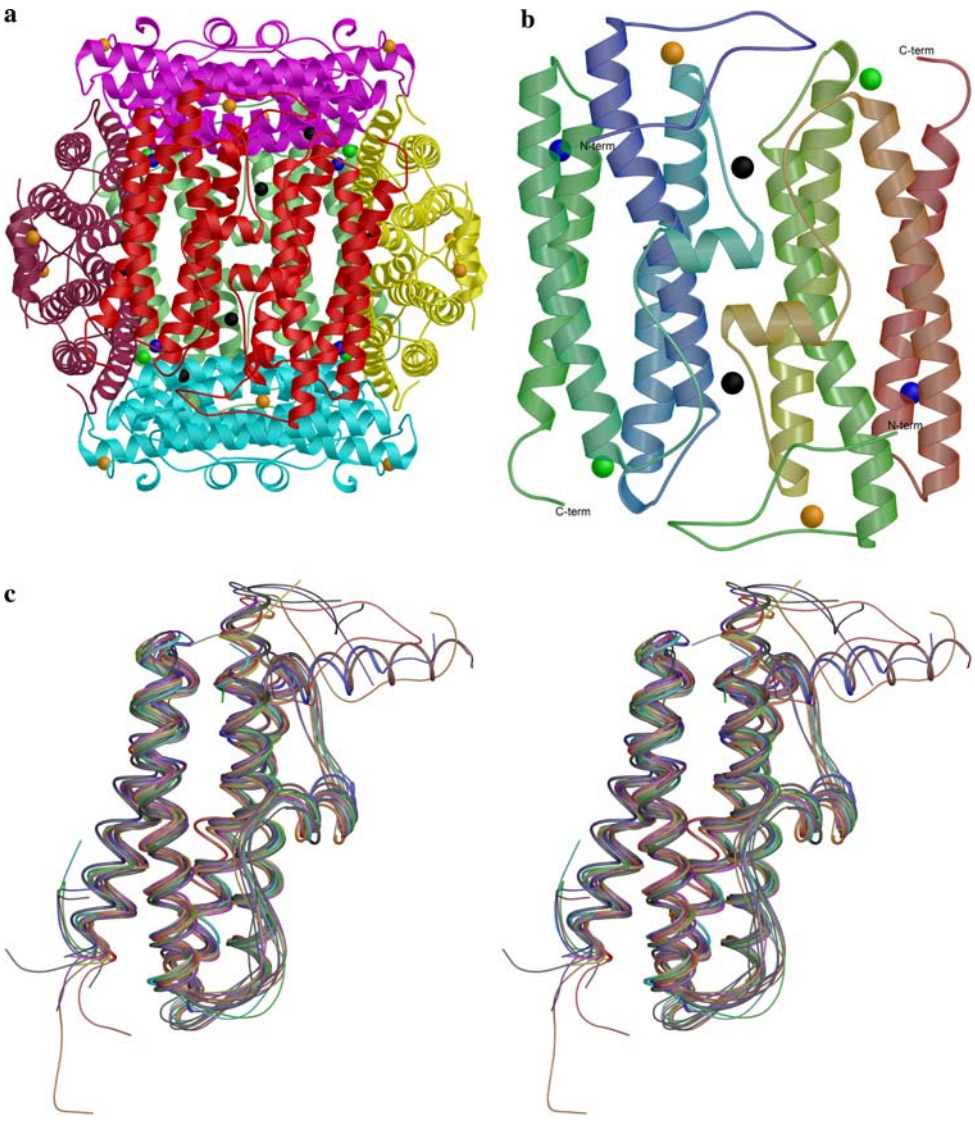

Fig. 1 **a** Overall view of DNA-binding protein from starved cells (*Dps*) DR2263 dodecamer structure along the twofold axis in structure B. The helices are represented as *ribbons* and each dimer is represented with a different colour. **b** Ribbon representation of the dimer in structure B: both monomers are represented with a rainbow scale colour. In both **a** and **b** the different metal sites are represented as spheres with different colours: *black* iron site corresponding to the ferroxidase iron centre; *blue* iron sites located in the threefold axis N-terminal pore; *green* iron sites located in the threefold axis C-terminal pore; *yellow* zinc site in the N-terminal extension. **c** Stereo view of the superposition of the Dps monomers from the proteins for which the crystallographic structure is published; *red* Dps DR2263, *blue* 1ZUJ, *brown* 1ZS3, *orange* 1TJO, *black* 1DPS, *cyan* 1UMN, *light green* 1VEQ, *violet* 1O9R, *yellow* 1N1Q, *dark green* 1QGH, *pink* 1JI5, *grey* 1JIG, *dark blue* 1JI4

Figure 1c was prepared with Swiss-PdbViewer [37], MolScript [38] and Raster3D [39].

Coordinates

Structure factors for the three data sets and associated structure coordinates were deposited in the Protein Data Bank [accession codes 2C2U (structure A) and 2C2F (structure B)].

Results and discussion

Overall structure

The Dps DR2263 crystal structure was determined in two forms: structure A to 1.1-Å resolution corresponding to the native protein form and structure B to 1.6-Å resolution from a native crystal soaked in an iron solution. Both crystals belong to space group *P*23, with unit cell parameter $a = 90.39$ Å (structure A) and 90.2 Å (structure B), containing one subunit per asymmetric unit. The quaternary Dps DR2263 structure is a dodecamer with 23 symmetry (Fig. 1a), composed of identical subunits and is similar to other members of the Dps family, for example those from *E. coli*, *Listeria innocua* and *Agrobacterium tumefaciens* [6, 7, 13]. The dodecamer displays a hollow, almost spherical, structure, and each subunit has a molecular mass of 23 kDa with 207 amino acid residues, consisting of a four-helix bundle and a short helix in the middle of the loop between helices B and C similar to other members of the Dps family (Fig. 1). Helix B in the four-helix bundle is kinked, owing to two consecutive amino acid residues: a phenylalanine and a proline (Phe106 and Pro107) in the middle of the helix.

These two residues are only present in this Dps DR2263 compared with the other Dps sequences (Fig. 2). The residue Phe106 from the twofold related subunits are close by: the distance between the CZ atoms from the two Phe106 residues in a Dps dimer is approximately 3.8 Å, and this hydrophobic environment is located in-between the two mononuclear iron ferroxidase centres.

A comparison of Dps monomer structures with Dps DR2263 reveals that the four-helix bundle is highly conserved and the main difference is located in the N-terminal extension (Figs. 1c, 2). Although in both structures presented here, the native form and the iron-soaked form, the first 29 amino acid residues were not modelled owing to disorder, the remaining 25 N-terminal residues before helix A define a loop that harbours a metal Zn centre (see later).

The N-terminal extension and the zinc site

A comparison of the Dps DR2263 sequence with other Dps sequences shows that both *D. radiodurans* Dps have a longer N-terminal, an extension of 53 amino acid residues before the start of the first helix of the four-helix bundle in the case of DR2263 (Fig. 2), compared with other known Dps. Both *D. radiodurans* proteins share only 17% of sequence identity (Fig. 2), though the tertiary and quaternary structures are

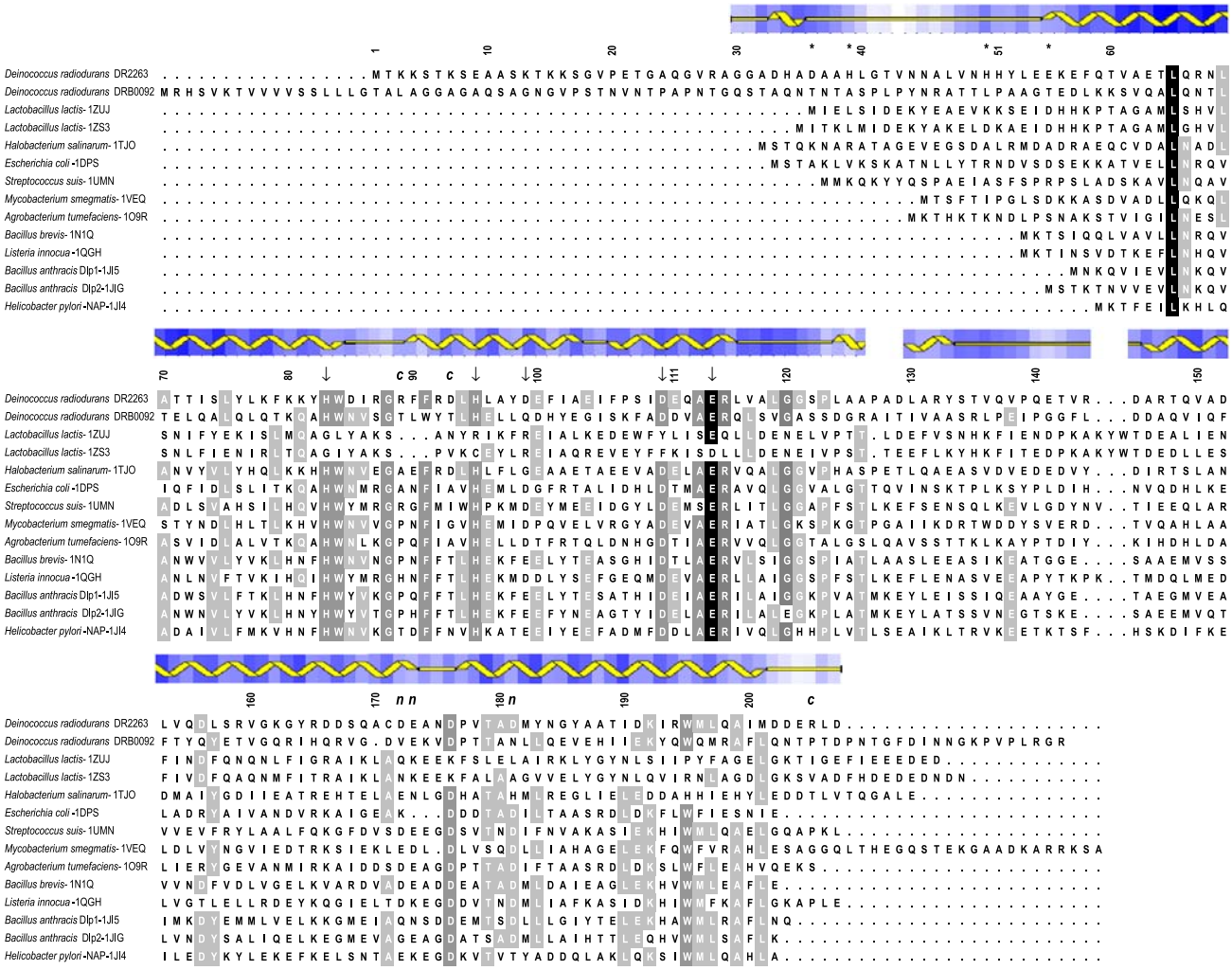

Fig. 2 Multiple amino acid sequence alignment of Dps proteins using ClustalX. The Dps DR2263 secondary structure is represented *above* the alignment. The amino acid residues involved in the iron ferroxidase centre are represented by an *arrow*; amino acid residue ligands of the zinc site are represented by an *asterisk*; amino acid residues involved in the threefold axis N-terminal pore are marked as *n*; amino acid residues involved in the threefold C-terminal pore are marked as *c*. The *black boxes* represent the strictly conserved residues, *dark grey boxes* represent most conserved residues and *light grey boxes* represent less-conserved residues among the selected sequences in Fig. 1c

highly conserved between these two proteins (M. Cuypers, personal communication) as well as in the Dps family members known so far. The sequence alignment also shows N-terminal extensions to occur in other Dps family members: *Halobacterium salinarum*, *E. coli*, *Streptococcus suis* and *Lac. lactis*, have shorter extension of 22–23 amino acids [6, 8, 10, 11], and *A. tumefaciens* and *M. smegmatis* have an even shorter N-terminal extension of only 10–11 residues before helix A [13, 15].

Dps DR2263 has a total of seven positively charged residues in the N-terminal extension (before residue 30) composed of six lysine residues and one arginine residue, with the following motif Lys3Lys4$(X)_2$-Lys7$(X)_5$Lys13(X)Lys15Lys16$(X)_{11}$Arg28. It was shown that Dps DR2263 in both the dimeric and dodecameric forms interact with DNA [26]. This DNA interaction could be through the N-terminal extension, in which the positively charged residues may have an important role. Indeed, in both of the crystallographic structures presented here, the electron density for the first 29 N-terminal residues was too poor to allow them to be modelled, indicating that this part of the N-terminal is flexible and may be involved in the DNA interaction.

Between residue 30 and before the start of helix A in Dps DR2263, there are still 23 amino acid residues and this region contains a zinc metal centre, tetrahedrally coordinated by two nitrogen bases from histidine residues (His39 and His50) and two carboxylate groups from one aspartate residue (Asp36) and one glutamate residue (Glu55) (Figs. 2, 3a). The binding motif for this zinc centre is Asp36$(X)_2$His39$(X)_{10}$His50$(X)_4$Glu55 and this is the first time that this type of metal centre has been observed in either the Dps or ferritin families. In fact, the amino acid sequence forming the ligands for this metal centre is unique to this Dps DR2263 when compared with the other Dps proteins presented in Fig. 2. In the dodecamer assembly, this zinc centre is located on the external surface of the sphere, accessible to the solvent (Fig. 3b), suggesting that the first 29 residues of the N-terminal extension are highly likely to be located on the external surface, both accessible to the solvent and available for DNA interactions.

In zinc-containing proteins, the role of the zinc ion may be catalytic, co-catalytic or structural. The metal can be coordinated by a variety of amino acid combinations, including nitrogen from histidine, oxygen from either aspartate or glutamate or even sulphur from cysteine [41]. The zinc coordination observed in Dps

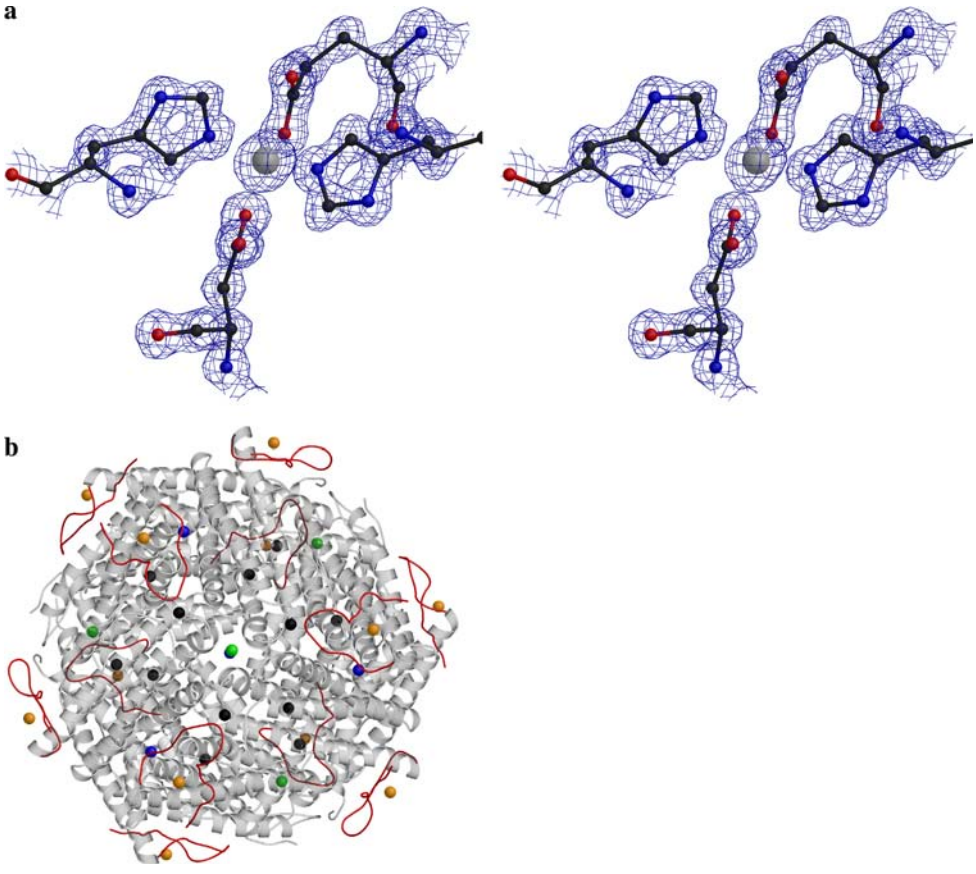

Fig. 3 **a** Stereo view of Dps DR2263 zinc site. View of the electron density in a $2|F_o - F_c|$ map contoured at 1.5σ in the vicinity of the zinc centre in structure A. Ligands, starting from the *top* and in *clockwise direction* are Glu55, His50, Asp36 and His39. The distances from the zinc to the ligands are 2.01 Å (Asp36, $O^{\delta 2}$), 2.01 Å (Glu55, $O^{\epsilon 2}$), 2.02 Å (His39, $N^{\epsilon 2}$) and 2.02 Å (His50, $N^{\epsilon 2}$). **b** View down the threefold axis of the dodecamer Dps DR2263; the N-terminal extensions are coloured in *red* and the four-helix bundles are coloured in *grey*. The different metal centres are represented as *spheres* and are coloured the same as for Fig. 1

DR2263, by two histidines, one glutamate and one aspartate residue, is present in the family members of prokaryotic metalloregulatory transcriptional repressors, the SmtB family, where the intersubunit zinc site α_5 functions as a metal sensor [42, 43]. Although the role of the Dps DR2263 zinc centre remains to be clarified, a possible function may be to stabilise the N-terminal extension in such a way that allows a proper orientation for DNA interaction. Another possibility is that it may function as a metal sensor, responding to stress conditions, or it may even be a zinc finger involved in interactions with DNA.

The intersubunit iron centres

As in the case of other Dps family members, Dps DR2263 has two identical monoiron ferroxidase centres, created by twofold rotational symmetry, with ligands from two different monomers (Fig. 1b) [7, 9, 13, 15, 19]. From both structures presented here, only structure B revealed a phased anomalous peak (49.7σ) corresponding to a ferroxidase iron centre in a position equivalent to that present in other members of the Dps family. This indicates that this protein is able to bind iron and possibly able to catalyse the oxidation of ferrous to ferric ion. In fact, it was shown that this protein has ferroxidase activity in vitro [26]. The distance between the two iron atoms related by the twofold intersubunit symmetry is around 24 Å (Fig. 1b). Each iron atom is octahedrally coordinated by three residues: a nitrogen from His83 from one subunit and carboxylate groups, Asp110 (bidentate) and Glu114 (monodentate), from the symmetry-related subunit (Fig. 4). Besides the protein ligands, the iron atom is also coordinated by two non-protein ligands, a water molecule and a hydroxy moiety of a glycerol molecule, which also forms hydrogen bonds with the amino acids Asp99 ($O^{\delta 2}\cdots$water, 2.62 Å) and His95 ($N^{\epsilon 2}\cdots$O2, 2.62 Å), respectively (Fig. 4). In the case of the Dps DR2263 structure A, there is no density that may be assigned to an iron atom at the position corresponding to the iron in structure B. However, it is quite interesting that in structure A both amino acid residues Asp110 and Glu114 were modelled with two alternate conformations, with 70 and 30% occupancies. In structure B, the conformation of both amino acid residues corresponds to the lower occupancy conformation of structure A, suggesting that in the native form some structural rearrangement of these residues is necessary in order to coordinate the iron.

The amino acids involved in the intersubunit iron ferroxidase centre of Dps DR2263 have the binding motif: $His83(X)_{11}His95(X)_3Asp99(X)_{10}Asp110(X)_3$-Glu114, with His95 and Asp99 bridged to the iron through a glycerol and water molecules, respectively (Fig. 4). The Dps DR2263 iron ferroxidase centre is octahedrally coordinated, which differs from the tetrahedral coordination present in other Dps proteins, for example *M. smegmatis* and *B. anthracis* [12, 15]. However, for *H. salinarum* DpsA, the crystals of which were soaked anaerobically in a ferrous solution, a hexagonally distorted iron coordination was observed with three protein residues, His52, Asp79 and Glu83, and two waters [11]. Dps DR2263 structure B and *H. salinarum* DpsA were obtained from a crystal soaked in a ferrous solution, suggesting that the change in the iron coordination from tetrahedral to octahedral is probably a result of the iron soaking process, in which an iron oxidation mechanism occurs.

Amongst the sequences presented in Fig. 2, this intersubunit iron motif is well conserved, apart from Asp99, where a glutamate is occasionally substituted. The two Dps from *Lac. lactis*, are a special exception to this motif conservation since they have only one iron

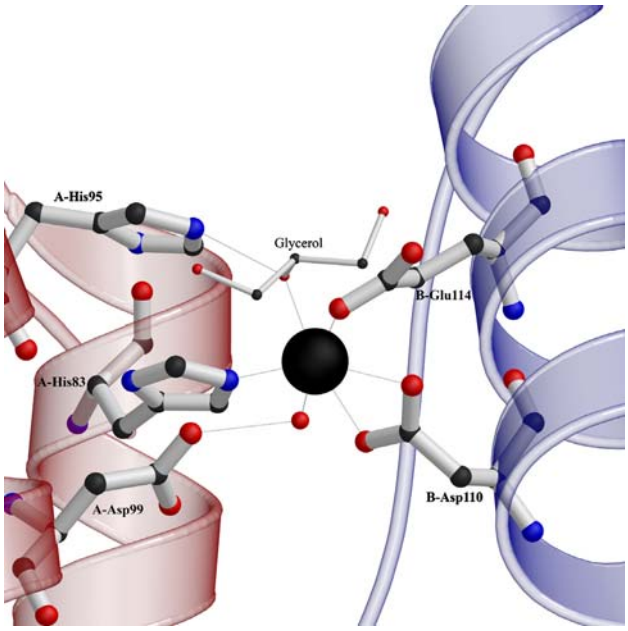

Fig. 4 Intersubunit ferroxidase iron centre of Dps DR2263 structure B. The iron is represented as a *black sphere*. The amino acid residues involved in the iron coordination are represented with the two subunits with different colours. Bond lengths from the iron and its ligands are as follows: from subunit A, 2.15 Å (His83, $N^{\epsilon 2}$); from subunit B, 2.37 and 2.30 Å (Asp110, $O^{\delta 1}$ and $O^{\delta 2}$, respectively), 2.00 Å (Glu114, $O^{\epsilon 1}$), 2.11 Å to a water molecule and 2.22 Å to a glycerol molecule O2. The bridging ligands, water and glycerol, are hydrogen-bonded to other neighbouring residues: His95 ($N^{\epsilon 2}$) forms a bifurcated hydrogen bond to two glycerol hydroxyl groups, O1 (2.61 Å) and O2 (2.81 Å) and Asp99 ($O^{\delta 2}$) forms a hydrogen bond to the water molecule (2.62 Å)

ligand present (Fig. 2) [8]. In the case of *H. salinarum* Dps, the only residue not conserved is Asp99, which is replaced by a glycine residue (Fig. 2) [11].

However, other Dps binding motifs for iron may exist. For example, the Dps-like protein from *Sulfolobus solfataricus* has ferroxidase activity, although it lacks the conventional iron binding motif, and an alternative possibility has been suggested [20].

The threefold-symmetry intersubunit sites

The 23 symmetry of the Dps dodecamer leads to two non-equivalent environments around the threefold axes and these are organised as pores, designated as the N-terminal and C-terminal pores. In the Dps DR2263 structure B, two peaks in the phased anomalous difference map could be identified at the internal end (i.e. towards the centre of the dodecamer) of both pores, while only one phased anomalous difference peak was identified for the native structure at the internal end of the C-terminal pore.

The N-terminal pore is highly hydrophilic, providing a strong negative electrostatic surface potential that might allow and encourage iron entry into the protein. This pore corresponds to the iron entry channel of mammalian and prokaryotic ferritins [44, 45]. In Dps DR2263 this channel can be described as having three layers of negatively charged residues, Glu173-Asp172-Asp181 (Fig. 5a). This pore is funnel-shaped, starting from the top (external edge of the sphere) with three symmetrically related glutamates (Glu173). The pore has a diameter (as inscribed by a circle between the oxygens $O^{\epsilon 1}$ and $O^{\epsilon 2}$ from the different residues) of around 10.0 Å. The layer below is defined by three aspartate residues, Asp172, with a diameter of 5.4 Å. In the third layer, closest to the internal sphere space, the pore narrows even further and is defined by three aspartate residues, Asp181, with a diameter of 3.0 Å. At this point in the pore, an anomalous peak of 34.4σ was identified for structure B. This peak was assigned to an iron atom resulting from the iron solution used to soak the crystal and therefore was refined as iron. This metal is coordinated octahedrally: by three oxygens ($O^{\delta 1}$) from the three symmetrically related aspartate residues with a distance of 2.1 Å and by three symmetrically related water molecules with a distance of 2.4 Å. The distance between the oxygen $O^{\delta 1}$ of the aspartate residue (Asp181) at the bottom end of the pore and the oxygen $O^{\epsilon 1}$ from the glutamate residue (Glu173) at the top of the entrance is around 15.9 Å. This pore, composed of these three layers of clusters of threefold symmetrically related acidic residues, may act as an entry point for ferrous ions in vivo. There are additionally two positively charged residues (Lys56 and Lys162) at the surface of the protein, around 15 Å distant from Glu173 at the top of the pore, which may

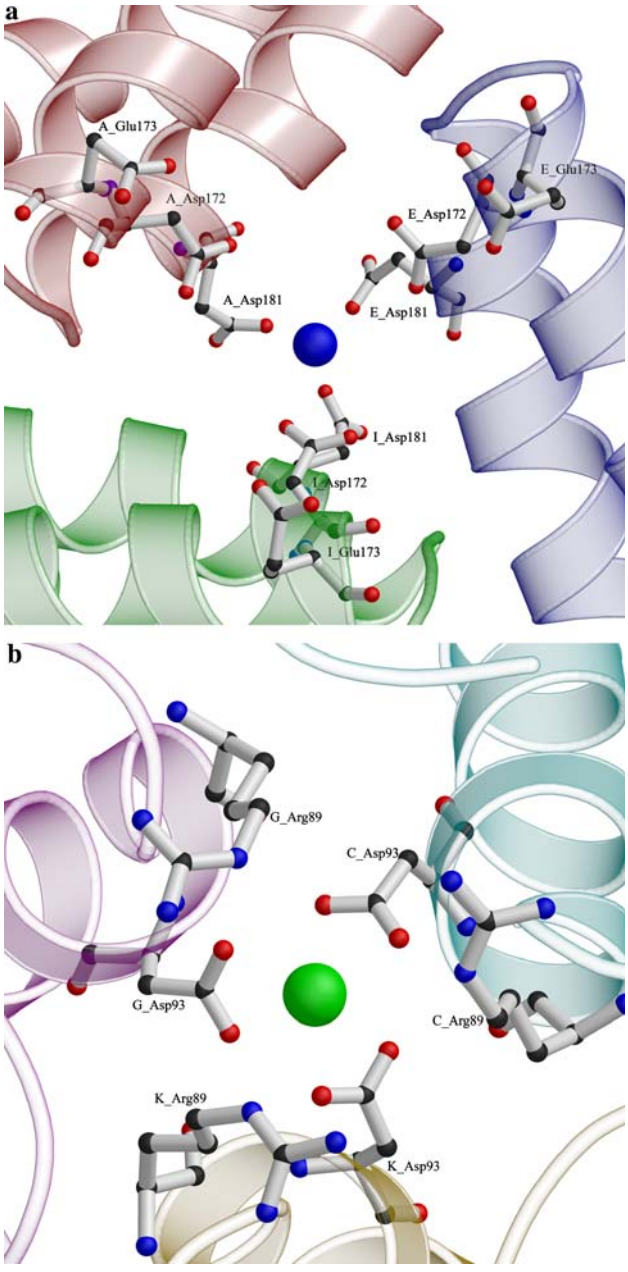

Fig. 5 The two types of threefold axis for Dps DR2263 for structure B. The subunits are drawn with different colours. **a** Threefold axis at the N-terminal pore; the iron is represented as a *blue sphere*. This pore is composed of three layers of three symmetry-related negatively charged residues from three symmetrically related amino residues: from the top Glu173, on the second layer Asp172 and then Asp181, which coordinates the iron. **b** Threefold axis at the C-terminal pore; the iron is represented as a *green sphere*. For this pore only the second layer corresponding to the positively charged residues Arg89 and then the negatively charged residues Asp93 that coordinate the iron atom are represented

function as an electrostatic guide for ferrous ion to the pore.

In structure A, the native form, no phased anomalous peak could be identified in an equivalent position, and residue Asp181 was modelled in two conformations, thereby showing some flexibility prior to iron binding. In the Asp181 conformer observed for the iron-soaked conformation, a water molecule is located 2.43 Å from $O^{\delta 2}$ of this residue in the equivalent position to the metal site found in structure B. The fact that this metal site is coordinated by only three protein ligands, the three symmetrically related aspartates, Asp 181, all monodentates, may indicate that this position is transiently occupied during the iron incorporation process.

The C-terminal pore is not present in the ferritin family of proteins and is unique to the Dps family members. In both the Dps DR2263 structures presented here a phased anomalous peak was observed inside the pore. For structure A the peak is 7.6σ and for structure B is 19.1σ. In both cases, an iron was refined on this position. In the case of the iron-soaked crystal the metal could come from the solution, although for structure A the nature and origin of this metal are not known; however, in both cases it is octahedrally coordinated by three symmetry-related aspartates, Asp93. In Dps DR2263 this channel can be described by the following sequence of amino residues from the outside to the inside of the dodecamer: Arg205-Arg89-Phe90-Asp93 (Fig. 5b). Starting from the entrance, this channel is defined by two layers of positively charged symmetry-related arginine residues (Arg205 and Arg89) (Fig. 5b) with a pore diameter of 4.4 Å for the Arg205 layer, and 6.4 Å for Arg89. In structure B, a sulphate ion is located between these two layers, and nitrogen atoms ($N^{\eta 2}$) from both arginine residues form hydrogen bonds with the sulphate oxygens. The layer below is hydrophobic, as it is formed by three symmetry-related phenylalanine residues (Phe90). The final layer is defined by three negatively charged aspartate residues (Asp93) which coordinate the metal as bidendate ligands. The metal is octahedrally coordinated with a distance of around 2.5 Å from both carboxylate groups from Asp93 in structure B and 2.6 Å in structure A. One glycerol molecule is located below this metal (at a distance of approximately 5 Å).

The C-terminal pore in Dps DR2263 in which there is a positively charge entrance may function as an iron exit channel, as opposed to the N-terminal pore entrance. Near the C-terminal pore Arg205 there are three symmetry-related carboxylate residues, Glu204, which may assist with iron exit. The fact that in both structures presented here, the native and the iron-soaked, a metal site was found to be coordinated by Asp93 may indicate that this site is always present.

The internal negative charge of the sphere is contributed to by various carboxylate residues: Asp99, Glu100, Glu104 and Glu111 from helix B. This cluster of negatively charged residues is present on some of the Dps proteins presented in Fig. 2, for example *L. innocua*. These residues are probably involved in the iron core nucleation, as was also proposed for the ferritin family as well as for the Dps from *L. innocua* [16, 44, 45]. Two of these residues are in close contact with two positive residues: Glu100···Arg92 and Glu104···Lys192. The interaction of these two positive Dps DR2263 residues, Arg92 and Lys192, forming salt bridges with the negative residues Glu100 and Glu104, is stronger in the native form than in the iron-soaked form, and probably indicates that in the iron incorporation mechanism both these negative residues could be more available for involvement in the iron core formation, whilst in the native structure these negative charges inside the cavity can be stabilised by these positive residues. It is interesting to note that in bacterioferritins from, for example, *E. coli* and *Desulfovibrio desulfuricans* the aspartate residue corresponding to the Glu104 in Dps DR2263 is also close to a positive residue: a lysine and an arginine residue for *E. coli* and *Desulfovibrio desulfuricans*, respectively [46–48].

Conclusions

D. radiodurans is a bacterium extremely resistant to DNA damaging conditions. This bacterium has two Dps-type genes in the genome and in this paper the crystal structure of one of this proteins, Dps DR2263, was presented. The quaternary overall structure formed by this type of protein is highly conserved: a dodecamer composed of four-helix bundle monomers. The principal structural difference among Dps proteins lies in the N-terminal or C-terminal tails, which may have an important role for the different cellular functions of each protein.

An important feature of this particular protein is the presence of a unique zinc metal centre at the N-terminal extension. From a structural point of view, the 12 zinc centres of Dps DR2263 are directed towards the external surface of the protein dodecamer. The function of this metal centre is not yet established, but could have a structural function, in such a way that the positively charged lysine and arginine residues on the N-terminal extension will interact with DNA. Another hypothesis is that it may function as a metal sensor.

Nevertheless, the actual biological function of this metal centre is currently under investigation.

The results presented here from structure B (the iron-soaked form) indicate that the iron entry into the protein sphere may be facilitated by the threefold N-terminal pore which has a negative electrostatic potential, and the negatively charged cluster of residues may help attract iron into the protein, allowing iron to be trapped by the three symmetrically positioned aspartate residues (Asp181). The presence of a mononuclear iron ferroxidase centre between the subunits, similar to other Dps members, shows that this protein has the potential for ferrous oxidation. The structure of the threefold C-terminal pore has positive residues at the top of the pore (on the outside of the sphere) and on the inside of the sphere ends on three symmetrical aspartate residues (Asp93), which were found to coordinate a metal ion in both forms, native (structure A) and iron-soaked (structure B). This suggests that this site could be permanently occupied and either may have only a structural function or may act as an iron exit, owing to its electrostatic potential, which could push positive charges to the outside of the sphere.

The results presented here for the structure of Dps DR2263 from *D. radiodurans* suggest a role in oxidative stress protection by being able to store iron and therefore protect the bacterium from the effects of free iron in the cell, and also provide a protective role through interaction with DNA in which the N-terminal could be involved. Further work is necessary in order to establish the actual cellular function of this Dps in normal bacterial growth and in the recovery mechanism after irradiation.

References

1. White O, Eisen JA, Heidelberg JF, Hickey EK, Peterson JD, Dodson RJ, Haft DH, Gwinn ML, Nelson WC, Richardson DL, Moffat KS, Qin HY, Jiang LX, Pamphile W, Crosby M, Shen M, Vamathevan JJ, Lam P, McDonald L, Utterback T, Zalewski C, Makarova KS, Aravind L, Daly MJ, Minton KW, Fleischmann RD, Ketchum KA, Nelson KE, Salzberg S, Smith HO, Venter JC, Fraser CM (1999) Science 286:1571–1577
2. Mattimore V, Battista JR (1996) J Bacteriol 178:633–637
3. Daly MJ, Gaidamakova EK, Matrosova VY, Vasilenko A, Zhai M, Venkateswaran A, Hess M, Omelchenko MV, Kostandarithes HM, Makarova KS, Wackett LP, Fredrickson JK, Ghosal D (2004) Science 306:1025–1028
4. Ghosal D, Omelchenko MV, Gaidamakova EK, Matrosova VY, Vasilenko A, Venkateswaran A, Zhai M, Kostandarithes HM, Brim H, Makarova KS, Wackett LP, Fredrickson JK, Daly MJ (2005) FEMS Microbiol Rev 29:361–375
5. Almiron M, Link AJ, Furlong D, Kolter R (1992) Genes Dev 6:2646–2654
6. Grant RA, Filman DJ, Finkel SE, Kolter R, Hogle JM (1998) Nat Struct Biol 5:294–303
7. Ilari A, Stefanini S, Chiancone E, Tsernoglou D (2000) Nat Struct Biol 7:38–43
8. Stillman TJ, Upadhyay M, Norte VA, Sedelnikova SE, Carradus M, Tzokov S, Bullough PA, Shearman CA, Gasson MJ, Williams CH, Artymiuk PJ, Green J (2005) Mol Microbiol 57:1101–1112
9. Zanotti G, Papinutto E, Dundon W, Battistutta R, Seveso M, Giudice G, Rappuoli R, Montecucco C (2002) J Mol Biol 323:125–130
10. Kauko A, Haataja S, Pulliainen AT, Finne J, Papageorgiou AC (2004) J Mol Biol 338:547–558
11. Zeth K, Offermann S, Essen LO, Oesterhelt D (2004) Proc Natl Acad Sci USA 101:13780–13785
12. Papinutto E, Dundon WG, Pitulis N, Battistutta R, Montecucco C, Zanotti G (2002) J Biol Chem 277:15093–15098
13. Ceci P, Ilari A, Falvo E, Chiancone E (2003) J Biol Chem 278:20319–20326
14. Ren B, Tibbelin G, Kajino T, Asami O, Ladenstein R (2003) J Mol Biol 329:467–477
15. Roy S, Gupta S, Das S, Sekar K, Chatterji D, Vijayan M (2004) J Mol Biol 339:1103–1113
16. Bozzi M, Mignogna G, Stefanini S, Barra D, Longhi C, Valenti P, Chiancone E (1997) J Biol Chem 272:3259–3265
17. Yamamoto Y, Poole LB, Hantgan RR, Kamio Y (2002) J Bacteriol 184:2931–2939
18. Zhao G, Ceci P, Ilari A, Giangiacomo L, Laue TM, Chiancone E, Chasteen ND (2002) J Biol Chem 277:27689–27696
19. Pulliainen AT, Kauko A, Haataja S, Papageorgiou AC, Finne J (2005) Mol Microbiol 57:1086–1100
20. Wiedenheft B, Mosolf J, Willits D, Yeager M, Dryden KA, Young M, Douglas T (2005) Proc Natl Acad Sci USA 102:10551–10556
21. Frenkiel-Krispin D, Levin-Zaidman S, Shimoni E, Wolf SG, Wachtel EJ, Arad T, Finkel SE, Kolter R, Minsky A (2001) EMBO J 20:1184–1191
22. Frenkiel-Krispin D, Ben-Avraham I, Englander J, Shimoni E, Wolf SG, Minsky A (2004) Mol Microbiol 51:395–405
23. Ceci P, Cellai S, Falvo E, Rivetti C, Rossi GL, Chiancone E (2004) Nucleic Acids Res 32:5935–5944
24. Wolf SG, Frenkiel D, Arad T, Finkel SE, Kolter R, Minsky A (1999) Nature 400:83–85
25. Liu Y, Zhou J, Omelchenko MV, Beliaev AS, Venkateswaran A, Stair J, Wu L, Thompson DK, Xu D, Rogozin IB, Gaidamakova EK, Zhai M, Makarova KS, Koonin EV, Daly MJ (2003) Proc Natl Acad Sci USA 100:4191–4196
26. Grove A, Wilkinson SP (2005) J Mol Biol 347:495–508
27. Powell HR (1999) Acta Crystallogr Sect D 55:1690–1695
28. CCP4 (1994) Acta Crystallogr Sect D 50:760–763
29. Winn MD (2003) J Synchrotron Radiat 10:23–25
30. Bricogne G, Vonrhein C, Flensburg C, Schiltz M, Paciorek W (2003) Acta Crystallogr Sect D 59:2023–2030
31. Murshudov GN, Vagin AA, Dodson EJ (1997) Acta Crystallogr Sect D 53:240–255
32. Murshudov GN, Vagin AA, Lebedev A, Wilson KS, Dodson EJ (1999) Acta Crystallogr Sect D 55:247–255
33. Jones TA, Zou JY, Cowan SW, Kjeldgaard M (1991) Acta Crystallogr Sect A 47(Pt 2):110–119
34. Laskowski RA, MacArthur MW, Moss DS, Thornton JM (1993) J Appl Crystallogr 26:283–291
35. Thompson JD, Gibson TJ, Plewniak F, Jeanmougin F, Higgins DG (1997) Nucleic Acids Res 25:4876–4882
36. Nicholas KB, Nicholas HBJ (1997) http://www.psc.edu/biomed/genedoc
37. Guex N, Peitsch MC (1997) Electrophoresis 18:2714–2723

38. Kraulis PJ (1991) J Appl Crystallogr 24:946–950
39. Merritt EA, Murphy ME (1994) Acta Crystallogr Sect D 50:869–873
40. Esnouf RM (1999) Acta Crystallogr Sect D 55:938–940
41. McCall KA, Huang C, Fierke CA (2000) J Nutr 130:1437S-1446S
42. Eicken C, Pennella MA, Chen X, Koshlap KM, VanZile ML, Sacchettini JC, Giedroc DP (2003) J Mol Biol 333:683–695
43. Busenlehner LS, Pennella MA, Giedroc DP (2003) FEMS Microbiol Rev 27:131–143
44. Harrison PM, Arosio P (1996) Biochim Biophys Acta 1275: 161–203
45. Theil EC (2001) Ferritin. Wiley, Chichester
46. Frolow F, Kalb AJ, Yariv J (1994) Nat Struct Biol 1:453–460
47. Macedo S, Romao CV, Mitchell E, Matias PM, Liu MY, Xavier AV, LeGall J, Teixeira M, Lindley P, Carrondo MA (2003) Nat Struct Biol 10:285–290
48. Carrondo MA (2003) EMBO J 22:1959–1968